Catalysis Letters Vol. 99, Nos. 3–4, February 2005 (© 2005)
DOI: 10.1007/s10562-005-2121-9

Catalytic oxidation of methane over novel Ce–Ni–O mixed oxide catalysts prepared by oxalate gel-coprecipitation

Nan Yisup, Yong Cao,* Wei-Liang Feng, Wei-Lin Dai and Kang-Nian Fan

Department of Chemistry & Shanghai Key Laboratory of Molecular Catalysis and Innovative Materials, Fudan University, Shanghai 200433, P.R. China

Received 15 October 2004; accepted 15 November 2004

A novel approach for the synthesis of a new type of binary Ce–Ni–O mixed oxide catalysts is reported. The synthesis method involves the homogeneous gel-coprecipitation of oxalate precursor in alcoholic solution followed by calcinations in air. The results show that the as-prepared samples have high specific surface area and high component dispersion, exhibiting remarkably high activity in the catalytic combustion of methane as compared to the catalysts prepared by conventional coprecipitation techniques. It is suggested that the superior catalytic performance of the oxalate gel-coprecipitated Ce–Ni–O mixed oxide catalysts could be attributed to the generation of highly dispersed NiO_x species and the creation of highly active oxygen vacancies as a consequence of an easier incorporation of Ni^{2+} ions into ceria lattice by the formation of solid solution in the mixed oxide samples.

KEY WORDS: catalytic combustion of methane; Ce–Ni–O mixed oxide catalyst; oxalate gel-coprecipitation; oxygen vacancy.

1. Introduction

Catalytic combustion of hydrocarbons offers the alternative possibility of being a promising process for environmentally benign energy production [1,2]. The significant advantages of catalytic combustion are a more efficient use of energy source with minimum pollutant emissions as compared to conventional flame combustion [3]. Particularly in the field of methane oxidation, light-off point (defined as 10% conversion of the fuel stream) should really be achieved at temperature of ca. 400 °C. Therefore, the development of new type of catalytic materials with attractive properties such as a high catalytic activity, low ignition temperature, long-term thermal stability and low cost are highly desirable [4].

The use of noble metals such as Pd or Pt dispersed on various supporting materials for catalytic combustion is well documented [5–7]. However, due to the severe operating conditions, these noble metals are frequently susceptible to sintering and formation of volatile compounds during catalytic combustion [8]. Recently, metal mixed oxide catalysts have been extensively investigated and recognized as active catalysts in a variety of catalytic processes such as the hydrocarbon oxidation [9,10]. Although they are generally less active than noble metals, they have the advantage that numerous active solid-state phases can be obtained. Among them, perovskite type oxides containing transition metals (e.g., Co, Cr, Mn, etc.) are considered of great interest for the combustion of hydrocarbon and NiO_x selective reduction. However, these materials usually possess particularly low specific surface areas, which greatly compromise their potential applications as practical catalysts [11,12].

On the other hand, cerium-based catalysts with the presence of transition metals have attracted increasingly attention in recent years due to their high oxygen storage capability (OSC) [13–16]. The important role of ceria played in catalytic reactions is suggested to be the generation and participation of surface oxygen species and anionic vacancies in the catalytic reactions [17]. A number of more recent studies have shown that these redox properties can be significantly enhanced if additional elements are introduced into ceria lattice by forming solid solutions [17–19]. Thus, various binary ceria-based catalysts [13–19] have been studied with the purpose of increase the thermal stability and OSC of the CeO_2. Particularly, it has been reported that the addition of NiO to the CeO_2 leads to improvements in its oxygen storage capacity and redox properties, providing new opportunity to develop new efficient mixed oxide catalyst system for the low temperature catalytic combustion of hydrocarbons [20–22].

In the present work, in an attempt to develop new efficient catalyst system for the catalytic oxidation of methane, the preparation of new type of Ce–Ni–O mixed oxide catalysts by a novel gel-coprecipitation of oxalate precursor as well as their performance in the

*To whom correspondence should be addressed.
E-mail: yongcao@fudan.edu.cn.

methane oxidation reaction is reported. The influence of the coprecipitation method on the catalytic behavior of the Ce–Ni–O catalysts is also investigated. The chemical and structural characterization of these catalysts has been carried out to establish the relationship between the catalytic performance and physicochemical properties such as the nature and dispersion of the NiO_x species in the catalysts. It is demonstrated that the oxalate gel-coprecipitation method, previously established to be an effective technique for the preparation of the highly efficient $Cu/ZnO/Al_2O_3$ methanol synthesis catalyst developed by our group [23], has shown to be particularly useful in optimizing the structural and surface redox properties of the Ce–Ni–O mixed oxide catalysts for the catalytic oxidation of methane.

2. Experimental

2.1. Catalyst preparation

The oxalate gel-coprecipitated Ce–Ni–O catalysts were prepared by following a modified procedure involving the gel-coprecipitation of oxalate precursor [23]. Briefly, two alcoholic solutions of mixed nitrates and 20% excess of oxalic acid were combined at room temperature under vigorous stirring. The resultant precipitate of oxalate was then recovered by centrifuge and then dried at 110 °C overnight, followed by calcination in air at 550 °C for 3 h. The as-prepared samples were referred as Ce_xNi_yO–OG, where x/y denotes the molar ratio of Ce to Ni.

For comparison, the pure CeO_2 and NiO oxides were prepared by decomposition of cerium nitrate and nickel nitrate at 650 °C and 500 °C, respectively. The reference samples denoted as Ce_xNi_yO–OC and Ce_xNi_yO–KC were prepared by aqueous oxalate coprecipitation and KOH coprecipitation methods, respectively. All catalysts were finally obtained by calcination in air at 550 °C for 3 h.

2.2. Catalyst characterization

The textural parameters have been measured using the BET method by N_2 adsorption and desorption at 77 K in a Micromeritics TriStar system. The X-ray powder diffraction (XRD) of the catalysts was carried out on a Germany Bruker D8Advance X-ray diffraction meter using nickel filtered Cu Kα radiation ($\lambda = 1.5418$ Å) in the 2θ range from 10 to 80°. Temperature-programmed reduction (TPR) spectra were obtained on a homemade apparatus loaded with 100 mg of catalyst. The samples were contacted with an H2/Ar mixture (H_2/Ar molar ratio of 5/95 and a total flow of 40 ml min^{-1}) and heated, at a rate of 5 °C min^{-1}, to a final temperature of 1000 °C. The H_2 consumption was monitored using a TCD detector. Laser Raman spectra were obtained using a confocal microprobe Raman system (LabRam Infinity, Dilor). The excitation wavelength was 514.5 nm from an internal Ar^+ laser with a power of 12 mW. Spectra were recorded with a resolution of 4 cm^{-1}.

2.3. Catalytic activity measurements

The catalytic oxidation of methane was carried out in a fixed-bed quartz microcatalytic flow reactor at atmospheric pressure with 100 mg catalyst (60–80-mesh) loading. To avoid undesired hot spots in the catalytic bed, the catalysts were diluted with 300 mg quartz powder (40–60-mesh). The feed was constituted of a mixture of CH_4/O_2/He with a molar ratio of 1/4/95 and a total gas flow of 24 ml/min, giving a space velocity (GHSV) of 27,000 h^{-1}. The feed and the product gases were analyzed on-line by a gas chromatograph (Type GC-122, Shanghai). Permanent gases (N_2, O_2, CO, CO_2) were separated using a TDX-01 column connected to a TCD detector and other reaction products were analyzed employing a Porapak Q column connected to a FID detector.

3. Results and discussion

3.1. Catalytic activity

The catalytic behaviors of the Ce–Ni–O mixed oxide catalysts prepared by gel-coprecipitation of oxalate precursor have been tested in the methane oxidation reaction and compared with the reference samples prepared by aqueous oxalate coprecipitation and KOH coprecipitation methods. In all cases, carbon monoxide is not formed and the selectivity is almost 100%. The remarkable catalytic combustion performance of the Ce–Ni–O catalysts prepared by the gel-coprecipitation of oxalate precursor can be seen from table 1. It is seen at the catalytic activity of the mixed catalysts is much higher than those of both pure ceria and pure nickel oxide. To obtain any given conversion between 10% and 80% with the pure oxides requires a temperature of ca. 50~100 °C higher than of the corresponding mixed oxides prepared by different methods. Table 1 summarizes the light-off temperatures and the half-conversion temperatures of the methane catalytic combustion. As far as the sample $CeNi_4O$–OG is concerned, it can real 50% conversion at ca. 150 °C lower than the single oxide of ceria and ca. 90 °C lower than pure nickel oxide.

Figure 1 shows the methane conversion as a function of temperature in the range 200–700 °C over the Ce–Ni–O mixed oxide catalysts derived from different methods with a Ni/Ce molar ratio of 4/1. As shown in figure 1, the light-off temperatures (T_{10}, defined as 10% conversion of methane) are at 267, 336 and 402 °C; and the half-conversion temperatures (T_{50}) at 406, 474 and 514 °C for the $CeNi_4O$–OG, the $CeNi_4O$–OC and the $CeNi_4O$–KC samples, respectively. This indicates a much higher catalytic activity for $CeNi_4O$–OG

Table 1
Physico-chemical properties and activity data for various Ce–Ni–O mixed oxide catalysts

Catalysts	S_{BET} (m^2/g)	T_{10}^a (°C)	T_{50}^b (°C)	T_{max}^c (°C)	Mean crystallite size (nm)[d]	Lattice parameter (Å)[e]
$CeNi_1O$–OG	64.1	290	427	333	6.1	5.419
$CeNi_2O$–OG	65.5	282	421	343	5.3	5.414
$CeNi_4O$–OG	67.9	267	406	354	4.7	5.408
$CeNi_6O$–OG	67.9	274	412	358	4.1	5.408
$CeNi_8O$–OG	58.9	280	419	363	2.6	5.405
$CeNi_4O$–OC	12.4	336	474	375	6.6	5.419
$CeNi_4O$–KC	16.1	402	514	394	11.5	5.421
CeO_2	39.0	388	560	–	15.3	5.430
NiO	4.6	348	492	–	–	–

[a] Temperature for 10% conversion of CH_4 to CO_2.
[b] Temperature for 50% conversion of CH_4 to CO_2.
[c] Temperature for the peak maximum in the TPR profiles.
[d] The mean crystallite size of cubic phase calculated from the Scherrer equation.
[e] The lattice parameters calculated by the square method according to the Cohen procedure [25].

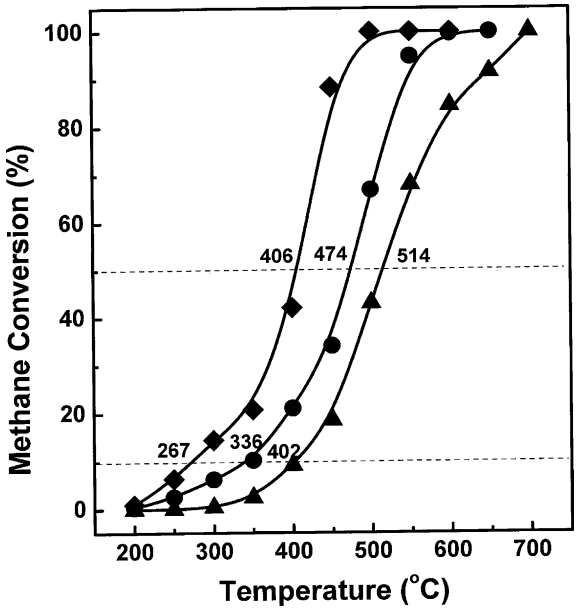

Figure 1. CH_4 conversion versus combustion temperature over (a) $CeNi_4O$–OG (♦); (b) $CeNi_4O$–OC (●), and (c) $CeNi_4O$–KC (▲).

compared to the reference samples. The variation of the methane conversion demonstrates that methane conversion depends strongly upon the preparation method. It is notable that I the overall activity of the present Ce_xNi_yO–OG sample is comparable with those of the noble metal catalysts (seen table 2) under the similar conditions, suggesting the superior performance of the $CeNi_4O$–OG as a highly active catalyst for the catalytic combustion of methane. In general, it is commonly accepted that the catalytic activity in light alkane combustion is proportional to the surface area and the amount of the incorporated active components [24]. One can see that BET specific surface area of the sample $CeNi_4O$–OG prepared by oxalate gel-coprecipitation methods is significantly higher than those prepared by the conventional precipitation methods. Thus, it is likely that the increased methane oxidation activity is strongly related to the much higher surface area achievable over the oxalate gel-coprecipitated samples.

Figure 2 displays the dependence of T_{50} and T_{100} (50% and 100% conversion of CH_4, respectively) as a function of Ni/Ce molar ratio. It is observed that the initial incorporation of NiO into ceria lattice results in a remarkable increase in the catalytic activity of methane combustion, as reflected from the sharp decrease in the T_{50} and T_{100} values for the Ce_xNi_yO–OG samples with molar ratio of Ni/Ce lower than 4/1. With further increasing Ni/Ce molar ratio, the half-conversion temperatures (T_{50}) and the total-conversion temperatures (T_{100}) of the Ce_xNi_yO–OG samples are observed to increase rapidly with respect to the $CeNi_4O$–OG sample. Thus, a much higher catalytic activity is achievable for $CeNi_4O$–OG compared to the samples with other Ni/Ce constitutions, demonstrating the presence of a strong synergy effect between the two components of ceria and NiO in the Ce_xNi_yO–OG systems.

3.2. Catalyst characterization

Table 1 summarizes the textural results for the Ce–Ni–O mixed oxide catalysts prepared by various methods. It is seen that the S_{BET} of the oxalate gel-coprecipitated catalysts is much higher than that of the reference samples prepared by aqueous oxalate coprecipitation and KOH coprecipitation methods. The results in table 1 clearly demonstrate that the combination of the Ce and Ni oxides greatly increased the specific surface area (S_{BET}) of the oxalate gel-coprecipitation derived materials. It is also notable that the lattice parameters of ceria decrease with the addition of Ni, suggesting that some Ni^{2+} ions are incorporated into the ceria lattice to form the solid solution of Ce_xNi_yO materials. Notice that the lattice parameter of ceria in the $CeNi_4O$–OG sample is much smaller than the reference samples of $CeNi_4O$–OC and

Table 2
The catalytic activity of various materials as indicated by temperatures for 50% combustion of methane (T_{50})

Catalysts	T_{50}^{a} (°C)	Reaction Conditions	References
1.0 wt% Pt/Al_2O_3	545	$CH_4(2\%)/O_2(10\%)/N_2$(Balance)	[5]
4.0 wt% Pt/Al_2O_3	495	$CH_4(2\%)/O_2(10\%)/N_2$(Balance)	[5]
1.0 wt% Pd/Al_2O_3	380	$CH_4(5\%)/O_2(20\%)/N_2$(Balance)	[6]
1.0 wt% Pd/ZrO_2	300	$CH_4(5\%)/O_2(20\%)/N_2$(Balance)	[6]
1.0 wt% Pt/CeO_2	617	$CH_4(1\%)/O_2(4\%)$/He(Balance)	[15]
LaCoO3	525	$CH_4(2\%)$/Air(Balance)	[11]
$LaMnO_3$	579	$CH_4(2\%)$/Air(Balance)	[11]
$Ce_{0.75}Zr_{0.25}O_2$	545	$CH_4(2\%)/O_2(21\%)$/He(Balance)	[14]
$Ce_{0.8}Hf_{0.2}O_2$	555	$CH_4(1\%)/O_2(4\%)$/He(Balance)	[15]
$Ce_{0.7}Ni_{0.3}O_2$	450	$CH_4(3\%)/O_2(8\%)/N_2$(Balance)	[22]
$CeNi_1O$–OG	427	$CH_4(1\%)/O_2(4\%)$/He(Balance)	This work
$CeNi_4O$–OG	406	$CH_4(1\%)/O_2(4\%)$/He(Balance)	This work

[a] Temperature for 50% conversion of CH_4 to CO_2.

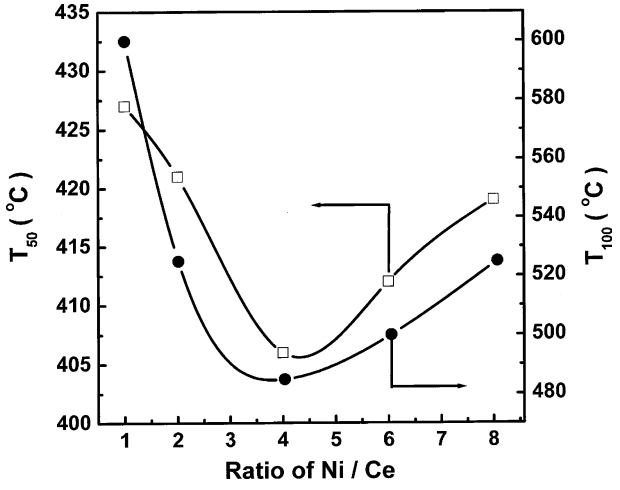

Figure 2. Temperature dependence for 50% and 100% conversion of CH_4 as a function of various Ni/Ce molar ratios.

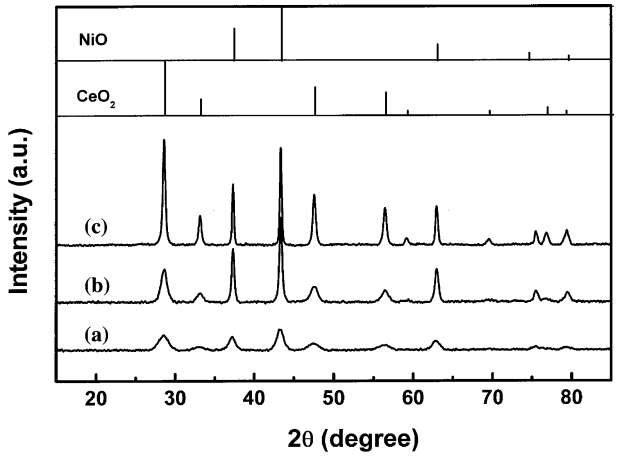

Figure 3. XRD patterns of the $CeNi_4O$ samples prepared by different methods: (a) $CeNi_4O$–OG; (b) $CeNi_4O$–OC; (c) $CeNi_4O$–KC.

$CeNi_4O$–KC, implying a higher amount of Ni^{2+} ions incorporated into ceria lattice could be achieved in the Ce_xNi_yO–OG catalyst systems as compared to those conventional catalysts [22]. For the Ce_xNi_yO samples prepared by the oxalate gel-coprecipitation method, the mean crystallite size of ceria was found to decrease with increasing Ni content, indicating that Ni atoms incorporated into CeO_2 inhibit the crystal growth of ceria. The same variation trend was evidenced for the lattice parameter of ceria in the Ce_xNi_yO–OG samples, suggesting that higher Ni content may result in higher amount of Ni incorporation into the ceria lattice.

Figure 3 shows the XRD patterns of the Ce–Ni–O mixed oxide catalysts prepared by various methods. For the sake of convenience, only the representative XRD patterns of for samples with Ni/Ce molar ratio of 4/1 are presented. For all three samples, the diffraction peaks corresponding to CeO_2 and NiO crystalline phases are observed. Note that the diffraction peaks corresponding to cerium and nickel oxides phases of the $CeNi_4O$–OG sample is much weaker and broader than those of $CeNi_4O$–OC and $CeNi_4O$–KC, indicating that the average particle size of the precipitates prepared by the present oxalate gel-coprecipitation method are much smaller than those of the conventional methods. Moreover, a red shift in the position near 28° of the diffraction peaks of CeO_2 in $CeNi_4O$–OG sample with respect to the diffraction patterns of the other samples and the JCPDS standard was identified. This further suggests the formation of Ce_xNi_yO solid solution in the bulk of the catalyst, in agreement with the previous observation of the formation of Ce_xNi_yO solid solution reported by Wrobel *et al.* [26–28]. Thus, the present XRD data show that at least two types of Ni phase existed in the Ce_xNi_yO samples, i.e., crystallized NiO phase dispersed on the surface of CeO_2, and Ni^{2+} ions incorporated into ceria lattice.

Figure 4 shows the H_2-TPR profiles of CeO_2, NiO and the $CeNi_4O$ mixed oxide samples prepared by various methods. There is a weak reduction peak at ca. 830 °C (δ_1)

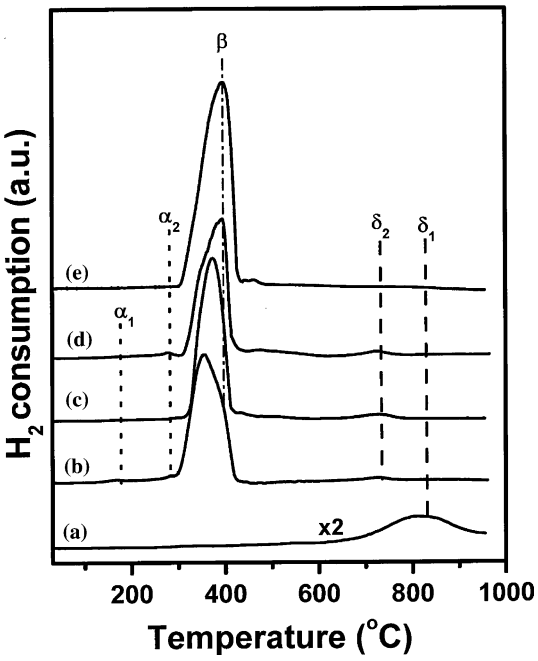

Figure 4. TPR profiles of the $CeNi_4O$ samples prepared by different methods:(a) CeO2; (b) $CeNi_4O$–OG; (c) $CeNi_4O$–OC; (d) $CeNi_4O$–KC; (e) NiO.

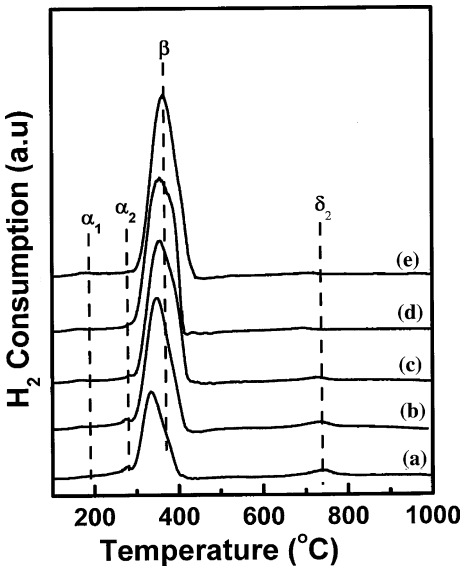

Figure 5. TPR profiles of the Ce_xNi_yO–OG samples prepared by the oxalate gel-coprecipitation method. (a) $CeNi_1O$–OG; (b) $CeNi_2O$–OG; (c) $CeNi_4O$–OG; (d) $CeNi_6O$–OG; (e) $CeNi_8O$–OG.

for pure CeO_2, which attributable to the reduction of crystalline CeO_2. As for the reduction of bulk NiO (see figure 4e), a single peak located at ca. 400 °C (β) associated with the reduction of crystalline NiO phase is observed. Remarkable profiles changes are identified for the reduction of $CeNi_4O$ mixed oxide samples prepared by various methods, where four hydrogen consumption peaks ($\alpha_1, \alpha_2, \beta$, and δ_2) are observed. The weak reduction peak (δ_2) ascribed to reduction of crystalline phase CeO_2 is shifted to a lower temperature of 735 °C in the $CeNi_4O$ mixed oxides, possibly due to the H_2-spillover effect as a consequence of the Ni incorporation [29]. The α_1 and α_2 peaks located at temperature range lower than 300 °C can be ascribed to the reduction of adsorbed oxygen species. It was generally accepted that the formation of the solid solution of Ce_xNi_yO by the incorporation of Ni^{2+} ions into ceria lattice would results in the generation of oxygen vacancies, leading to the formation of active oxygen species reducible by H_2 at low temperature. It is also seen that the main reduction peak corresponding to Ni species is centered at temperature of ca. 354 °C for $CeNi_4O$–OG, and those of $CeNi_4O$–OC and $CeNi_4O$–KC at ca. 375 °C and ca. 394 °C, respectively. Coupled with the BET data, the shift of the reduction maximum toward lower temperature with respect to other samples suggests the highly dispersed nature of the Ni species in the $CeNi_4O$–OG sample.

To gain a further insight into the effect of nickel incorporation on the reduction behavior of the mixed oxide samples prepared by the oxalate gel-coprecipitation method, figure 5 presents the H_2-TPR profits of the Ce_xNi_yO–OG catalysts with Ni/Ce molar ratio from 1/1 to 8/1. Again, four hydrogen consumption peaks labeled as $\alpha_1, \alpha_2, \beta$, and δ_2 are observed for all samples. The relative intensity of α_1 and α_2 peaks do not change obviously with increasing of Ni/Ce molar ratio from 1/1 to 8/1. This fact further confirms that only small amounts of Ni^{2+} ions can be incorporated into CeO_2 to form solid solution for low or high Ni content. One can also see that with increasing nickel oxide incorporation, the main reduction maximum is continuously shifted from 334 K for the $CeNi_1O$–OG sample to a higher temperature at 365 K for the $CeNi_8O$–OG sample. This observation further confirms the presence of three types of NiO phase in the Ce_xNi_yO–OG samples with high Ni content, where crystallized nickel oxide, solid solution and NiO phase highly dispersed on CeO_2 co-exist. Note that aggregate NiO phase on the surface of CeO_2 dominates for all Ce_xNi_yO–OG samples.

Laser Raman spectroscopy has been employed to elucidate the molecular nature of the Ce–Ni–O mixed oxide materials prepared by various methods. Figure 6 shows the Raman spectra of Ce–Ni–O samples prepared by various methods and pure compounds of CeO_2 and NiO. In pure CeO_2 (*Fm*3*m* space group), the intense band assigned to *F*2g mode is observed at 460 cm^{-1} [30]. For pure NiO, one strong broad band at ca. 1080 cm^{-1} as well as three we bands at ca. 688, 528, and 350 cm^{-1} associated with the NiO phase is identified [31]. It is seen that the spectra of all three mixed oxide samples with Ni/Ce molar ratio of 4/1 are featured by one strong band at ca. 440 cm^{-1}, which shifts to lower frequencies by ca. 20 cm^{-1} with respect to that of pure CeO_2, suggesting a significant modification of M–O bonding

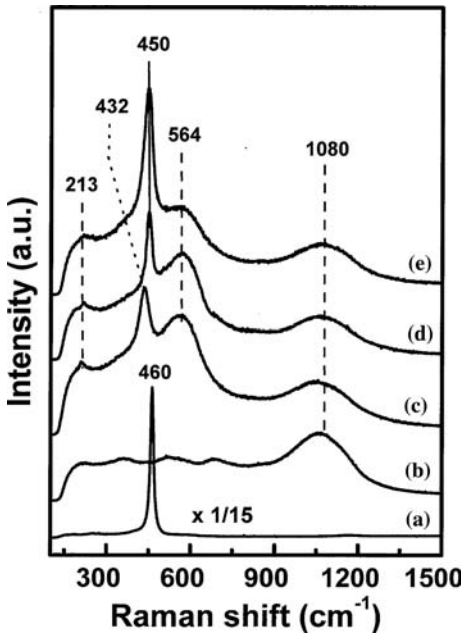

Figure 6. Raman spectra of pure oxides of CeO_2, NiO and $CeNi_4O$ samples prepared by different methods:(a) CeO_2; (b) NiO; (c) $CeNi_4O$–OG; (d) $CeNi_4O$–OC; (e) $CeNi_4O$–KC.

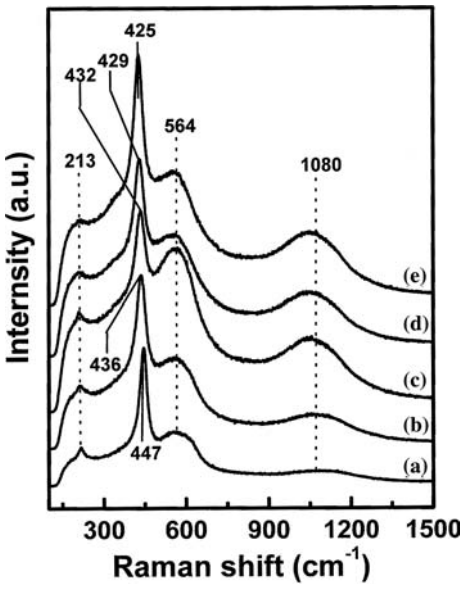

Figure 7. Raman spectra for the Ce_xNi_yO-OG samples with different Ni/Ce ratio (a) $CeNi_1O$-OG; (b) $CeNi_2O$-OG; (c) $CeNi_4O$-OG (d) $CeNi_6O$-OG; (e) $CeNi_8O$-OG.

symmetry in the mixed oxide catalysts. Although the identification of the broad band at 1080 cm^{-1} associated with the NiO phase suggests presence of crystallized NiO phase in all samples, the observation of the two additional weak bands at ca. 213 cm^{-1} and 564 cm^{-1} further confirms the formation of solid solution of by incorporation of Ni^{2+} ions into the ceria lattice. In addition, a variation the relative intensity for the two broad bands at ca. 213 and 564 cm^{-1} with respect to the sharp band at ca. 440 cm^{-1} attributed to the ceria lattice is identified in all three samples, suggesting a progressive modification of the M–O bonding symmetry [32]. Note that the relative intensity for the two broad bands at ca. 213 and 564 cm^{-1} relative to the sharp band at ca. 440 cm^{-1} are the strongest in the $CeNi_4O$–OG catalyst, pointing to the incorporation of higher amount of nickel into the ceria lattice with respect to the other two samples of $CeNi_4O$–OC and $CeNi_4O$–KC.

To further investigate the influence of the nickel incorporation on the molecular nature of the present oxalate gel-coprecipitated samples, the Raman spectra of the Ce_xNi_yO–OG samples with various Ni/Ce molar ratios were recorded. Figure 7a shows the Raman spectrum of the $CeNi_1O$–OG samples that exhibits spectroscopic features at ca. 213, 447, 564 and 1080 cm^{-1}. The shift of the ceria lattice *F*2g mode toward lower frequencies with respect to that of the pure ceria as well as the appearance of well-defined bands at 213 cm^{-1} and 564 cm^{-1} suggests the formation of solid solutions of CeO_2-NiO mixed oxide by incorporation of small amount of Ni^{2+} ions into the ceria lattice. Note that the road band at 1080 cm^{-1} ascribed to crystallized NiO phase is very weak, suggesting the formation of highly dispersed NiO species over the surface of $CeNi_1O$–OG sample. With the increase in nickel content, the intensity of the band at 1080 cm^{-1} increases with the nickel content (Figure 7b–e). Accompany the observation of the increased Raman bands associated with bulk NiO, the Raman feature at ca. 440 cm^{-1} corresponding to the ceria lattice *F*2g mode is red-shifted from 447 cm^{-1} to 425 cm^{-1} as the molar ratio of Ni/Ce is increased. This observation further demonstrates that the amount of Ni^{2+} ions incorporated into ceria lattice is strongly influenced by the Ni/Ce molar ratio in the Ce_xNi_yO–OG samples, in excellent agreement with the lattice parameter data presented in table 1.

In our experiments, the Ce_xNi_yO–OG catalysts obtained by gel-coprecipitation of oxalate precursor have demonstrated a unique catalytic behavior in methane combustion reaction as compared to the catalysts prepared by other methods. It is remarkable that a light-off temperature as low as at 267 °C is achieved over the $CeNi_4O$–OG catalyst. We have experimentally demonstrated that the present oxalate gel-coprecipitation method can allow the incorporation of substantially higher amount of nickel ions into the ceria lattice with respect to those conventional methods. In a recent investigation by Shan *et al.* it was reported that the $Ce_{1-x}Ni_xO_2$ ($x \leq 0.5$) mixed oxide catalysts prepared by sol-gel method show high activities for CH_4 oxidation [22]. The performance of the $Ce_{1-x}Ni_xO_2$ catalysts has been attributed to the highly dispersed Ni species and the more active oxygen species formed in the mixed oxides. Particularly, it was demonstrated that the highest amount of incorporated Ni^{2+} ions is achievable

over the $Ce_{0.7}Ni_{0.3}O_2$ sample, while either lower or higher Ni content can only result in the incorporation of less amount of Ni^{2+} ions into CeO_2 lattice in the ceria-rich mixed oxide samples. It is important to note that the present binary Ce_xNi_yO-OG mixed oxide samples have been investigated at the Ni-rich regions. In our case, an increasing amount of Ni^{2+} ions could be incorporated into the ceria lattice with increasing Ni/Ce molar ratio from 1/1 to 8/1. Therefore, the present oxalate gel-coprecipitation method may be particularly useful for preparing complexed mixed oxide systems with high component dispersion.

4. Conclusion

We describe the synthesis of a new type of binary Ce–Ni–O mixed oxide catalysts by homogenous gel-coprecipitated of oxalate precursor in alcoholic solution. These materials yield high surface area and high component dispersion, exhibiting remarkably high catalytic activity in the complete methane oxidation as compared to the catalysts prepared by conventional coprecipitation techniques. Combined XRD, TPR and Raman results demonstrated that the superior catalytic performance of the oxalate gel-coprecipitated Ce–Ni–O mixed oxide catalysts could be attributed to the generation of highly dispersed NiO_x species as well as the creation of higher concentration of active oxygen vacancies due to an easier incorporation of Ni^{2+} ions into ceria lattice by the formation of solid solution in the mixed oxide samples.

Acknowledgments

This work was supported by the National Nature Science Foundation of China (Grant No. 20473021, 20203003), the National Major Basic Research Program of China (Grant No. 2003CB615807), and the Committee of Shanghai Science and Technology (Grant No. 02QA14006).

References

[1] D.L. Trimm, Catal. Today 26 (1995) 231.
[2] M.F.M. Zwinlkels, S.G. Jarans and P.B. Menon, Catal. Rev. Sci. Eng. 35 (1993) 319.
[3] G. Saracco, G. Scibilia, A. Iannibello and G. Baldi, Appl. Catal. B 8 (1996) 229.
[4] D. Trong On, S.V. Nguyen and S. Kaliaguint, Phys. Chem. Chem. Phys. 5 (2003) 2724.
[5] R. Burch and P.K. Loader, Appl. Catal. B 5 (1994) 149.
[6] S.W. Yang, A. Maroto-Valiente, M. Benito-Gonzalez, I. Rodriguez-Ramos and A. Guerrero-Ruiz, Appl. Catal. B 28 (2000) 223.
[7] K. Sekizawa, K. Eguchi, H. Widjaja, M. Machida and H. Arai, Catal. Today 28 (1996) 245.
[8] V. Labalame, E. Garbowski, N. Guilhaume and M. Primet, Appl. Catal. A 138 (1996) 93.
[9] M.D. Fokema and J.Y. Ying, Catal. Rev. Sci. Eng. 43 (2001) 1.
[10] A.J. Zarur and J.Y. Ying, Nature 403 (2000) 65.
[11] H. Arai, T. Yamada, K. Eguchi and T. Seiyama, Appl. Catal. A 26 (1986) 265.
[12] M.A. Pena and J.L.G. Fierro, Chem. Rev. 101 (2001) 1981.
[13] R.K. Usmen, G.W. Graham, W.L. Warkins and R.M. McCabe, Catal. Lett. 30 (1995) 53.
[14] S. Pengpanich, V. Meeyoo, T. Rirksomboon and K. Bunyakiat, Appl. Catal. A 234 (2002) 221.
[15] F. Iamar, A. Trovareli, C. DeLeitenbury and G. Dolcetti, Chem. Commum. (1995) 965.
[16] G. Avgouropoulos, T. Loannides, H.K. Matralis, J. Batista and S. Hocevar, Catal. Lett. 73 (1) (2001) 33.
[17] J. Kaspar, P. Fornasiero and M. Grazini, Catal. Today 50 (1999) 285.
[18] F. Fally, V. Perrichon, H. Vidal, J. Kaspar, G. Blanco, J.M. Pintado, S. Bernal, G. Colon, M. Daturi and J.C. Lavalley, Catal. Today 59 (2000) 373.
[19] M. Daturi, E. Finocchio, C. Binet, J. Clavalley, F. Fally, V. Perrichon, H. Vidal, N. Hichey and J. Kaspar, J. Phys. Chem. B 104 (2000) 9186.
[20] L. Jalowiecki-Duhamel, A. Ponchel, C. Lamonier, A.D. Huysser and Y. Barbaux, Langmuir 17 (2001) 1511.
[21] H.S. Potdar, H.S. Roh, K.W. Jun, M. Ji and Z.W. Liu, Catal. Lett. 84 (2002) 95.
[22] W.J. Shan, M.F. Luo, P.L. Ying, W.J. Shen and C. Li, Appl. Catal. A 246 (2003) 1.
[23] Q. Sun, Y.L. Zhang, H.Y. Chen, J.F. Deng, D. Wu and S.Y. Chen, J. Catal. 167 (1997) 92.
[24] S.J. Cho, K.S. Song, I.S. Ryu, Y.S. Seo, M.W. Ryoo and S.K. Kang, Catal. Lett. 58 (1999) 63.
[25] H.P. Klug and L.E. Alexander, *X-Ray Diffraction Procedures*, (Wiley, New York, 1954).
[26] M.S. Sohier, G. Wrobel, J.P. Bonnel and J.P. Marcq, Appl. Catal. A 84 (1992) 169.
[27] G. Wrobel, M.P. Sohier, A. D'Huysser, J.P. Bonnelle and J.P. Marcq, Appl. Catal. A 101 (1992) 741.
[28] G. Wrobel, M.P. Sohier, A.D. Huysser and J.P. Bonnelle, Appl. Catal. A 101 (1993) 73.
[29] T. Takeguchi, S. Furukawa and M. Inoue, J. Catal. 202 (2001) 14.
[30] M. Thammachart, V. Meeyoo, T. Rirksomboon and S. Osuwan, Catal. Today 68 (2001) 53.
[31] R.E. Dietz, G.I. Parisot and A.E. Meixer, Phys. Rev. B 4 (1971) 2302.
[32] J.R. Mcbride, K.C. Hass, B.D. Poindexter and W.H. Weber, J. Appl. Phys. 76 (1994) 2435.